AD-A260 630

## NTATION PAGE

iverage 1 hour per response, including the time for reviewing instructions, searching existing data sources, gathering and
f information. Send comments regarding this burden or any other aspect of this collection of information, including suggestions
ate for Information Operations and Reports, 1215 Jefferson Davis Highway, Suite 1204, Arlington, VA 22202-4302, and to
'04-0188), Washington, DC 20503.

1. Agency Use Only *(Leave blank)*.	2. Report Date. 1993	3. Report Type and Dates Covered. Final - Proceedings

4. Title and Subtitle.
Sound Scattering from Submerged Elastic Objects and Shells of General Shape

6. Author(s).
Michael F. Werby, Russel D. Miller*, Gerard Maze**, Jean Ripoche**,
Xiao-Ling Bao*** and Herbert Uberall***

5. Funding Numbers.
Contract

Program Element No.	0601153N
Project No.	03202
Task No.	340
Accession No.	DN255011
Work Unit No.	12212B

7. Performing Organization Name(s) and Address(es).
Naval Research Laboratory Detachment
Ocean Acoustics and Technology Directorate
Stennis Space Center, MS 39529-5004

**DTIC
ELECTE
S FEB 2 4 1993 D
C**

8. Performing Organization Report Number.
PR 92:104:22?

9. Sponsoring/Monitoring Agency Name(s) and Address(e
Naval Research Laboratory Detachment
Ocean Acoustics and Technology Directorate
Stennis Space Center, MS 39529-5004

10. Sponsoring/Monitoring Agency Report Number.
PR 92:104:221

11. Supplementary Notes.
Published in Computational Acoustics, IMACS.
*NKF Engineering, Arlington, VA 22203, ** University of Le Havre, France, ***Catholic University of Americia.
Washington, DC 20064

12a. Distribution/Availability Statement.
Approved for public release; distribution is unlimited.

12b. Distribution Code.

13. Abstract *(Maximum 200 words)*.

Three computational approaches have been used to obtain backscattering amplitudes for sound waves incident on elastic objects and shells in water: the T-matrix method, the Finite element/Boundary element method, and the Superposition method. These methods have been found appropriate for analyzing the resonance effects apparent in the scattering from spheroidal solids, as well as from cylindrical shells with flat endcaps. The resonances have been interpreted by the phase matching of circumferential waves, and a simple method for obtaining the resonance frequencies based on the phase matching principle [H. Uberall, L. R. Dragonette, and L. Flax, J. Acoust. Soc. Am. 61, 711 (1977)] has proved suitable for predicting the calculated resonances of spheroids.

14. Subject Terms.
Acoustic scattering, shallow water, waveguide propagation

15. Number of Pages.
13

16. Price Code.

17. Security Classification of Report. Unclassified	18. Security Classification of This Page. Unclassified	19. Security Classification of Abstract. Unclassified	20. Limitation of Abstract. SAR

DISCLAIMER NOTICE
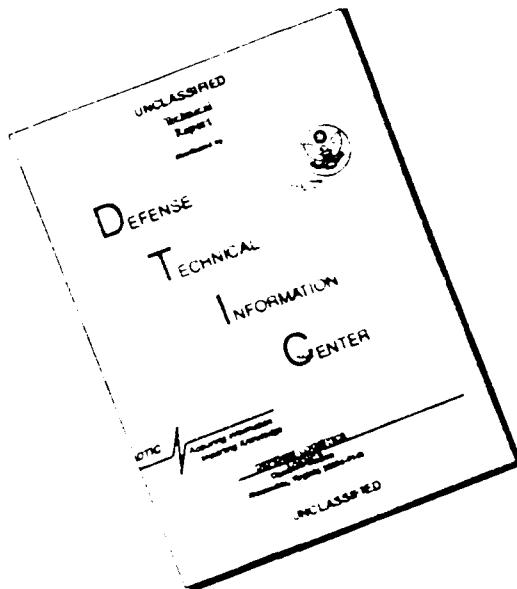
THIS DOCUMENT IS BEST
QUALITY AVAILABLE. THE COPY
FURNISHED TO DTIC CONTAINED
A SIGNIFICANT NUMBER OF
PAGES WHICH DO NOT
REPRODUCE LEGIBLY.

Sound Scattering from Submerged Elastic Objects and Shells of General Shape

Michael F. Werby   Russel D. Miller
NOARL (NRL)   NKF Engineering
Stennis Space Center, Mississippi 39529   Arlington, Virginia 22203

Gérard Maze and Jean Ripoche   Xiao-Ling Bao and Herbert Überall
LAUE--URA   Department of Physics
University of Le Havre   Catholic University of America
Le Havre 76610, France   Washington, DC 20064

Abstract: Three computational approaches have been used to obtain backscattering
amplitudes for sound waves incident on elastic objects and shells in water: the T-matrix
method, the Finite element/Boundary element method, and the Superposition method. These
methods have been found appropriate for analyzing the resonance effects apparent in the
scattering from spheroidal solids, as well as from cylindrical shells with flat endcaps. The
resonances have been interpreted by the phase matching of circumferential waves, and a
simple method for obtaining the resonance frequencies based on the phase matching principle
[H. Überall, L. R. Dragonette and L. Flax. J. Acoust. Soc. Am. 61, 711 (1977)] has proved
suitable for predicting the calculated resonances of spheroids.

I. INTRODUCTION

This paper describes the procedures used, and results obtained, computational as
well as experimental, in our studies of the acoustic scattering from a variety of submerged
elastic objects: solid elastic spheres, finite spheroids, as well as air-filled cylindrical shells of
finite length. In this investigation, we shall primarily concentrate on the resonances that
appear in the backscattering amplitude when plotted vs. frequency, for various purposes.
First, the resonances carry with them a wealth of information about the consistency and the
shape of the scattering object, which can for example be used for target classification
purposes [1]. Here, it will be shown that the resonance spacing for scattering from solid
spheroids can be used to determine the shear speeds of the medium the spheroids are made
of.

Second, the resonances are known to be caused by circumferentially propagating
surface waves (which are generated by the incident acoustic wave) that close into themselves
and, when they match phases, experience a resonant build-up by constructive interference
[2]. This picture provides physical insight into the scattering process, and allows us to
determine the properties of the surface waves that can exist on submerged solids. Conversely, if the surface wave speeds are known, a prediction of the resonance frequencies is

DTIC QUALITY INSPECTED 3

93-03877

93   2 23 123

possible depending on the shape of the object, and using a closed geodesic propagation path for the surface waves appropriate to the direction of incidence of the acoustic wave [3]. As an application of this method, resonance frequencies and surface wave dispersion curves were determined for solid spheroids and for cylindrical shells with hemispherical encaps.

While the above-described resonance calculations for spheroids were carried out using the NOARL T-matrix code [4], another numerical approach is utilized in our analysis of scattering experiments from finite-cylindrical shells with flat endcaps, namely the finite element/boundary element method, and also the superposition method as developed and/or extended by one of us (R.D.M.) [5]. Results of this method are compared with the experiments, and are physically interpreted via the dispersion curves of Lamb-type waves propagating on the shell, leading to the identification of the resonances by their generation of shell waves. Finally, calculated resonances of spheroids at axial incidence (the configuration used for the previously-mentioned examples) are shown to be to some extent observable also for broadside incidence, which casts light on the generation mechanism of the surface waves causing the resonances.

2. ACOUSTIC RESONANCES OF SOLID SPHEROIDS (MOSTLY AXIAL INCIDENCE)

The NOARL T-matrix code, as described earlier [4], was used to obtain the far-field backscattering amplitude ("form function") for plane waves axially incident on solid spheroids of various materials immersed in water: brass (Br), nickel (Ni), aluminum (Al), steel (St), molybdenum (Mo), and tungsten carbide (WC). Their material properties are listed in table 1; sound speed in water is taken as $c_0 = 1.4825$ m/s. Figure 1 shows the modulus of the form function of a prolate brass spheroid with aspect ratio 3:1 plotted vs. the reduced frequency $kL/2$ (k = sound wave number in water, L = length of spheroid), shown as a dashed line. It is well known, and this indeed forms the basis of the Resonance Scattering Theory (RST) [6], that the scattering amplitude is the superposition of a geometrical-reflection amplitude, and of a resonant sum of surface-wave amplitudes. For solid objects, the geometrical amplitude is closely enough represented by that of a rigid object of the same shape, and by coherently subtracting the latter, we obtain the pure resonance amplitude as a solid line in Fig. 1. The resonances are caused here by the phase matching of Rayleigh-type surface waves propagating along a meridian, labeled as Br_n, where n is the number of standing wavelengths around the path.

In Fig. 2, we show the resonance response for 3:1 spheroids of the six materials listed in table 1, and in Fig. 3 the resonance response for 6:1 spheroids. This allows us to observe the shifts in the resonance frequencies as to their dependence on the scatterer's material (and on the aspect ratio). Table 2 lists the resonance frequency ratios (normalized to brass) for the various materials, resonance orders n, and the two aspect ratios. Also listed are the ratios of the shear speed relative to that of brass. One notices a close agreement of these ratios (while the ratios of the p-wave velocities are found completely unrelated to the resonance ratios). It is seen, therefore, that the observed resonance positions may serve to

determine the material of the scattering object via its shear speeds -- an example of "inverse scattering" where the scattering object is identified by analyzing the acoustic echoes. And, since the resonances are generated by the phase matching of surface waves on the scattering object, this example also shows that the phase speeds of the surface waves are closely related to the bulk shear speeds in the material of the objects over which the surface waves propagate.

Table 1. Density ρ, p-wave speed c_p and shear wave speed c_s of spheroid materials.

	$\rho(g/cm^3)$	$c_p(m/s)$	$c_s(m/s)$
Br	8.9	4,400	1,900
Ni	8.7	6,000	3,000
Al	2.7	6,350	3,050
St	7.7	5,950	3,240
Mo	10.1	6,350	3,650
WC	13.1	6,950	3,940

Table 2. Resonance frequency ratios from Figs. 2 and 3, and
shear speed ratios relative to brass

n	2	3	4	2	3	4	c_s/c_s (Brass)
Ni	1.50	1.52	1.55	1.51	1.53	1.53	1.58
Al	1.53	1.53	1.55	1.54	1.54	1.63	1.60
St	1.59	1.63	1.67	1.63	1.62	--	1.70
Mo	1.78	1.82	--	1.79	1.81	--	1.92
WC	1.94	1.98	--	1.96	1.95	--	2.07

We finally show in a "level diagram" for WC spheroids for various aspect ratios (Figure 4) how the Rayleigh wave resonances shift (gradually) upwards with increasing aspect ratio [3] In addition, higher-order resonances (the so-called Whispering Gallery resonances) which manifest themselves by very narrow spikes, are shown also, labeled b a second index ℓ = 2,3,... (besides the first index n). They are seen to shift much more rapidly upward with aspect ratio, thereby crossing over the Rayleigh resonances (a phenomenon called "level crossing").

Figure 5 gives an example of both axial (a) and broadside incidence (b) on a 4:1 nickel spheroid. The form function (a) shows the n = 2 Rayleigh peak at $ka/2 = 7.0$, caused by the phase matching of a meridionally propagating Rayleigh wave. The same peak also appears at broadside incidence (b), indicating that even in this case, meridional waves are generated (while generally the surface waves generated here propagate equatorially around the object). This generating mechanism is illustrated in Figure 6 on the example of a hemispsherically-endcapped cylinder as discussed recently [7].

Resonance frequencies can be predicted by the phase matching condition

$$\int k_\ell \; ds = 2(n + 1/2)\pi, \tag{1}$$

where n is the number of wavelengths the ℓth surface wave type spans over the closed path (the extra $1/2$ being caused by phase jumps when the surface waves pass the two caustics). Knowing the (dispersive) wave number k_ℓ allows a determination of the resonance frequencies from Eq. (1); if k_ℓ is unknown, a simple "tangent sphere" model has been developed [8,9] where the known wave number on a sphere is used locally, the sphere being tangent to the object's surface along the propagation direction.

For the case of solid spheroids, this approach has been used in order to predict the resonance frequencies shown in Fig. 4, as discussed earlier [3]; it is also applicable to the results of Fig. 5.

3. ACOUSTIC RESONANCES ON HOLLOW CYLINDERS WITH FLAT ENDCAPS (AXIAL INCIDENCE)

This problem was analyzed using the Finite Element/Boundary Element Method, or the Superposition method, as described by us earlier [5]. We consider the end-on scattering from a cylindrical aluminum shell with flat circular-plate endcaps. Dimensions are $L = 30$ mm, $a = 9$ mm, shell thickness = 1 mm. An axisymmetric model of the shell was developed using the NASTRAN/SIERRAS code. The NASTRAN structural finite element model of the cylinder, after Guyan reduction, contained 160 grid points. The azimuthal increment of the axisymmetric model was two degrees.

The calculated backscattered form function for the end-on incidence of the cylindrical shell with flat endcaps is presented in Figure 7. The measured structural response spectra are also given in Figure 7. The experimental data were obtained at the University of Le Havre. The frequency and number of resonances observed by NASTRAN/SIERRAS and experiment are in reasonable agreement..The interpretation of the resonances is provided using the NASTRAN/SIERRAS results as follows:

In order to identify the resonances, the structural velocity and phase on the surface was examined for each peak and dip in the form function. Each peak in the form function indicates a frequency where the structure is strongly excited. This has been interpreted by the phase matching condition [2,10] (PMC) which associates the resonance condition with the waves ·· hich traverse the structure and return to the path origin in phase. Identification of the resonance is aided by an understanding of form function interpretation. As explained in earlier papers [11]. the width of the resonance provides an indication of the damping present in the mode being excited. Consider the first peak in the form function of Figure 7. The narrow width indicates that there is little damping in this first resonance. Since structural damping was ignored in this analysis. the only damping present is due to the fluid. The real part of the structural velocity for this case is depicted in Figure 8. The mode is easily recognized as the end fire (or "oil-canning") mode corresponding to the first mode of

the circular plate. Note that the response of the two endcaps is very similar for this mode. At this low frequency, the response of the fluid is largely reactive and it essentially sloshes from one end of the cylinder to the other and back over each cycle. Therefore, the fluid response is largely incompressible at this frequency and nodal cancellation over the entire body is large. Consequently, the reactive resistance is large, and the radiation efficiency, radiation damping and width of resonance are all small.

The time progression response plot over a complete cycle for the third peak (ka = 2.26) is shown in Figure 9. The curves shown in the figure were generated by computing the velocity response at ten different times and superimposing them onto a single plot. The endcap is responding with the m = 1 nodal line mode and the cylinder with the n = 3 half-waves longitudinal bending wave along the cylinder. The relatively large response for this mode is due to several factors. First, it is the frequency which excites the first single nodal line mode of the endcap. Second, the n = 3 mode of the cylinder is odd, leading to imperfect nodal cancellation over the cylindrical portion. Finally the two endcaps are in phase so that the contributions from the ends are additive.

The behavior of the shell at the peaks in the form function varies depending on the frequency. The coincidence frequency of the plating occurs at 228.3 kHz. At this frequency, the bending wavelength in an infinite plate is approximately the same as that in the fluid. Below this frequency the modes are easily identified (as in Figure 9). At and above coincidence, the behavior of the shell is not as well defined. Consider the time progression curve at ka = 19.8 shown in Figure 10. It is clear that no standing wave is observable here. The large radiation damping and wave interaction due to transmission and reflections at the discontinuities add complexity at these frequencies. It is difficult to assign a particular mode to the response due to the phasing of the velocity over the surface. However, an attempt was made to determine the primary wave traveling on the shell. The number of wavelengths was determined by counting the number of lobes along the cylinder as a function of time. The dominant number of half-waves along the cylinder for all times was used to compute the phase velocity.

The dispersion curve for aluminum was used to identify the wave types on the cylindrical shell. A comparison between the NASTRAN/SIERRA phase velocities for the finite shell with flat plate endcaps and the infinite plate dispersion curves is given in Figure 11. From the figure it is determined that the waves on the cylinder are positively identified as the Lamb "A" wave (pseudo-Stoneley, or fluid-borne wave [11]) Note that the dispersion curve rises again as the frequency approaches zero. This effect has been found previously for the spherical shell [11] and is primarily due to membrane effects (stretching) which dominate at the lower shell resonances. The fact that the phase velocity as determined by the method described in the preceding paragraph fits the dispersion curve so well tends to verify the identification method used.

The time progression plots are found to be useful and provide insight into the physical interpretation of the structural response. At low frequencies (well below coincidence), the incident wave envelops the structure and the behavior at the near and far

endcaps is similar in response (Figures 8 and 9). Near coincidence, the characteristic features are different. In Figure 10 it is observed that the near endcap is most strongly excited. Also, the longitudinal bending waves along the cylindrical shall begin with small amplitude and build up along the length of the cylinder. This is due to the fact that pressure is a scalar and excites the cylinder even though the velocity is parallel to it. Observe that the reflection at the far end of the cylinder results in an increase in amplitude near the far end. Further, there is an increase in response near the caustic point at the center of the far endcap. However, as the frequency has increased well above coincidence, shadowing on the far endcap is observable. The apparent modes of the near and far endcaps become different, which may be attributed to the difference in the types of loadings for the two ends at high frequency. The loading of the near endcap is primarily due to the incident wave, and therefore has relatively small in-plane excitation. The far endcap, on the other hand, has a large in-plane excitation due to the traveling axisymmetric wave on the cylinder stretching the far endcap. The shadowed side of the cylinder is excited primarily through the "corner" (actually an edge) which results in a "creeping wave" along the far endcap. Also, a large caustic point response is noted.

The large peak at $ka = 21.1$ in the structural response spectrum of Figure 7 is due to the $n = 6$ Lamb symmetric S_0 mode of the cylinder. This corresponds to a dip in the form function. This mode was clearly identified by observing the phase plots of the in-plane structural velocities and phase. This mode was the only dip which has a well defined phase change plot associated with it. Also, the peak in the structural response spectra is characteristic of S_0 responses [12].

4.   CONCLUSIONS

The end-on (and also broadside) acoustic resonance scattering from submerged finite-length cylindrical shells and spheroids has been analyzed by a T-matrix code, by the phase matching method, and by a finite element/boundary element calculation. Identification of the surface wave types, and physical interpretation of the results has been performed. Comparison with experimental results indicates that the resonances are of the correct spacing with respect to frequency. An example for the solution of an inverse problem has been presented, and the generation of meridionally propagating surface waves at broadside incidence has been demonstrated.

REFERENCES

[1] Überall, H., Inverse scattering and acoustic resonance spectroscopy, Traitement du Signal 2, No 5 sp., 1985, pp. 479-484.

[2] Überall, H., Dragonette, L. R., and Flax, L., Relation between creeping waves and normal modes of vibration of a curved body, J. Acoust. Soc. Am., vol 61, 1977, pp. 711-715.

[3] Werby, M. F., Castillo, J. J., Nagl, A., Miller, R., D'Archangelo, J.M , Dickey, J. W., and Überall, H.,Acoustic resonance spectroscopy for elastic spheroids of varying aspect ratios, and the level crossing phenomenon, J. Acoust. Soc. Am., vol. 88, 1990, pp. 2822-2829.

[4] Werby, M. F., and Green, L.H., An extended unitary approach for acoustical scattering from elastic shells immersed in a fluid, J. Acoust. Soc. Am., vol. 74, 1983, pp. 625-630; M. F. Werby and G. J. Tango, Numerical study of material properties of submerged elastic objects using resonance response, J. Acoust., Soc. Am., vol. 79, 1986, pp. 1260-1268.

[5] Miller, R. D., Moyer, E. T., Jr., Huang, H., and Überall, H., A comparison between the boundary element method and the wave superposition approach for the analysis of the scattered fields from rigid bodies and elastic shells, J. Acoust. Soc. Am., vol. 89, 1991, pp. 2185-2196.

[6] Flax, L., Dragonette, L. R., and Über   ...i., Theory of elastic resonance excitation by sound scattering, J. Acoust. Soc. Am   . ...3, 1978, pp. 723-731.

[7] Bao, X. L., Schumacher, C.R., anu Jberall, H., Complex resonance frequencies in acoustic-wave scattering from impenetrable spheres and elongated objects, J. Acoustic. Soc. Am., vol. 90, 1991, pp. 2118-2123.

[8] Merchant, B. L., Nagl, A., Stoyanov, Y. J., Überall, H., Brown, S. H,. and Dickey, J.W., Resonant phase matching of surface waves on impenetrable spheroids. J. Acoust. Soc. Am., vol. 80, 1986, pp. 1754-1756.

[9] Überall, H., Stoyanov, Y. J., Nagl, A., Werby, M. F., Brown, S. H., Dickey, J. W., Numrich, S. K., and D'Archangelo, J. M.,Resonance spectra of elongated objects, J. Acoust., Soc. Am., vol. 81, 1987, pp. 312-315.

[10] Überall, H., Moser, P. J., Merchant, B. L., Nagl, A., Yoo, K.B., Brown, S. H., Dickey, J. W., and D'Archangelo, J. M., Complex acoustic and electromagnetic resonance frequencies of prolate spheroids and related elongated objects and their physical interpretation. J. Appl. Phys., vol. 58, 1985, pp. 2109-2124.

[11] Talmant, M., Überall, H., Miller, R. D., Werby M. F., and Dickey, J. W., Lamb waves and fluid-borne waves on water-loaded, air-filled thin spherical shells. J. Acoust. Soc. Am., vol. 86, 1989, pp. 278-289.

[12] Miller, R.D., A comparison between the boundary element method and the superposition method for the analysis of the scattered fields from rigid bodies and elastic shells, D. Sc. dissertation, The George Washington University, University Microfilms International, 1990.
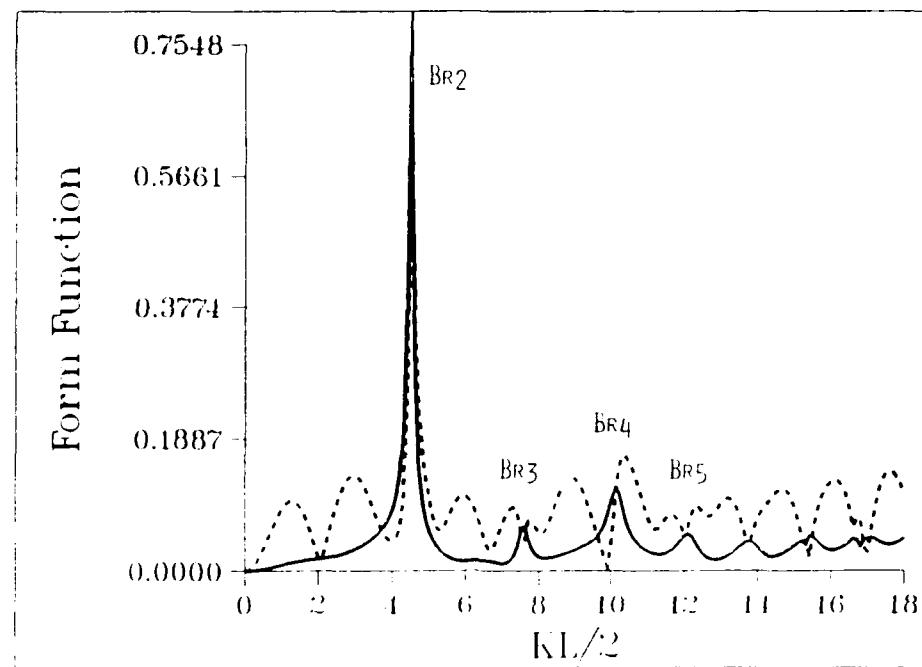
Fig. 1 Form function (dashed curve) and resonance response (solid curve) of a 3:1 *brass spheroid* under axial incidence of an acoustic plane wave. Resonances are labeled Br_n.

Residual Response VS. KL/2
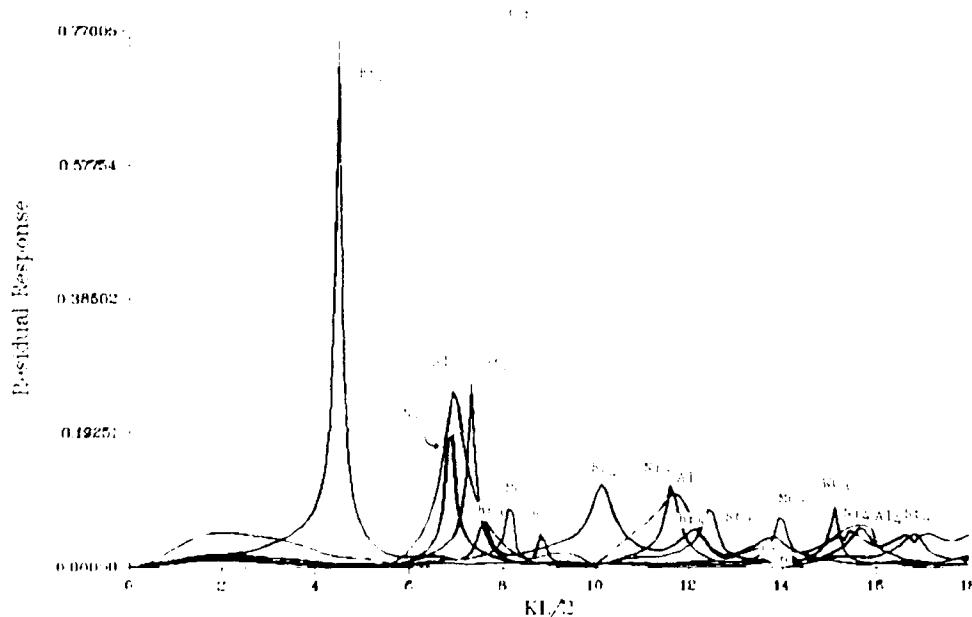
Fig. 2. Superimposed resonance response curves for 3:1 spheroids of the six materials of Table 1.

Residual Response VS. KL/2
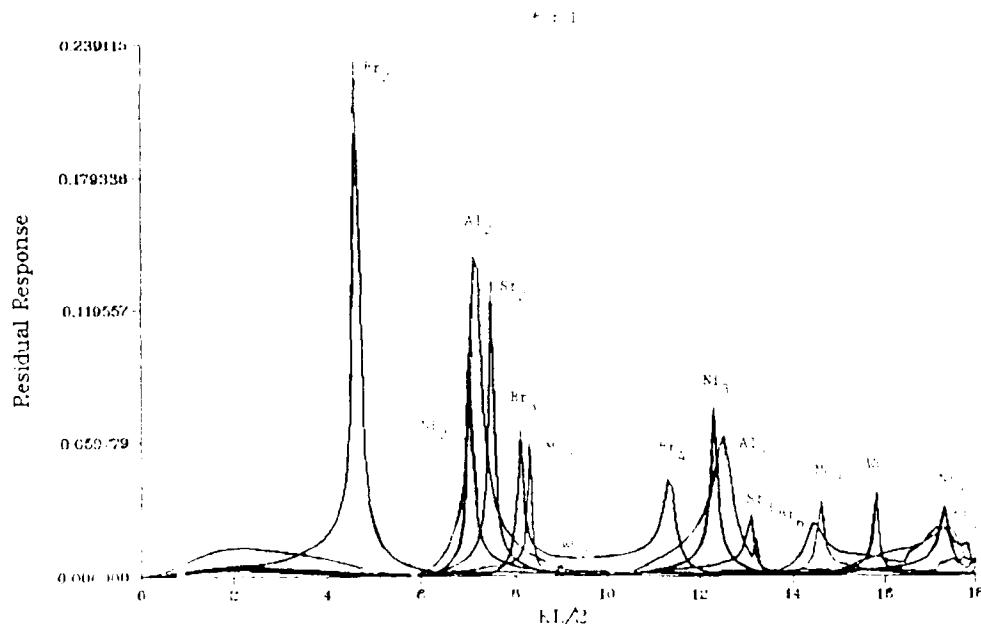
Fig. 3 Same as Fig. 2. for 6:1 spheroids.
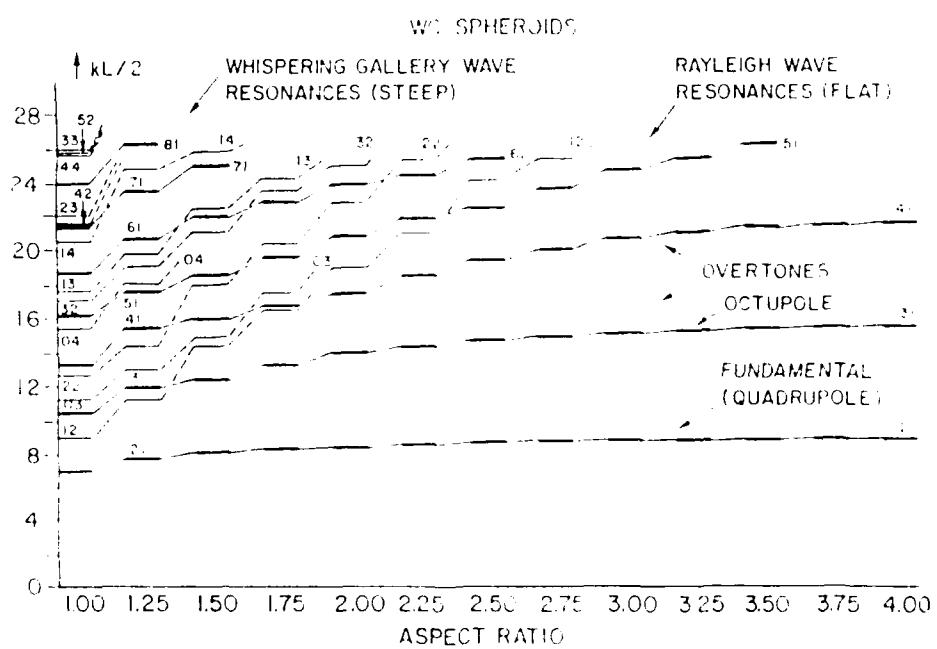
Fig. 4. Level diagram of Rayleigh and Whispering Gallery wave resonances
on WC spheroids as a function of aspect ratio.
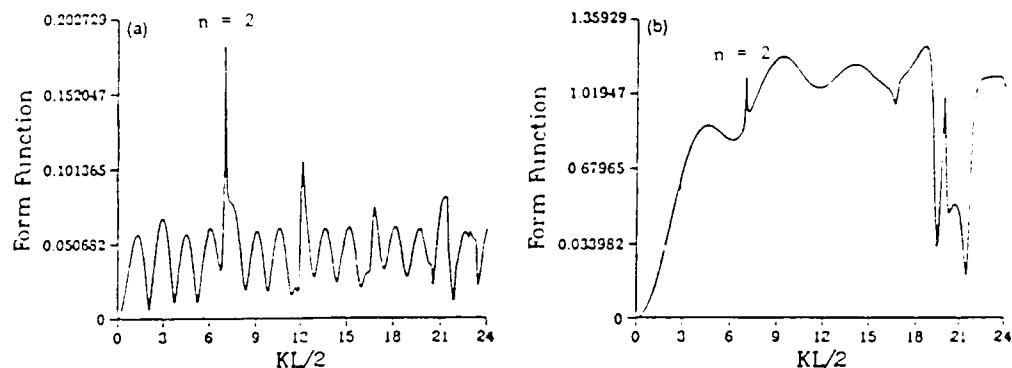
Fig. 5. Form function vs. kL/2 for 4:1 nickel spheroid: (a) axial incidence,
(b) broadside incidence.
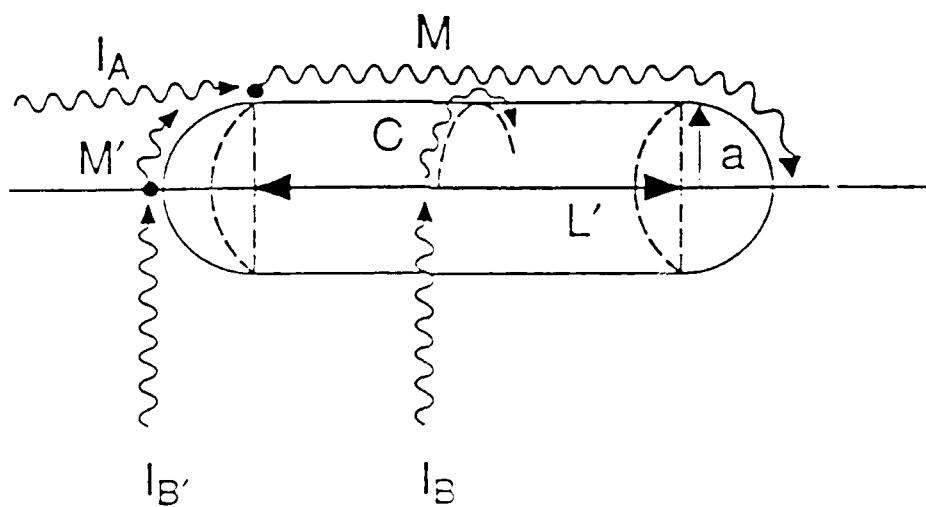
Fig. 6. Physical mechanism of meridional-wave resonance generation
upon broadside incidence.

Fig. 7. Backscattering form function (theoretical) and structural response spectra (experimental, with linear bias removed) for an aluminum cylindrical shell with flat-plate endcaps (L/D = 1.667, b/a = 0.889).
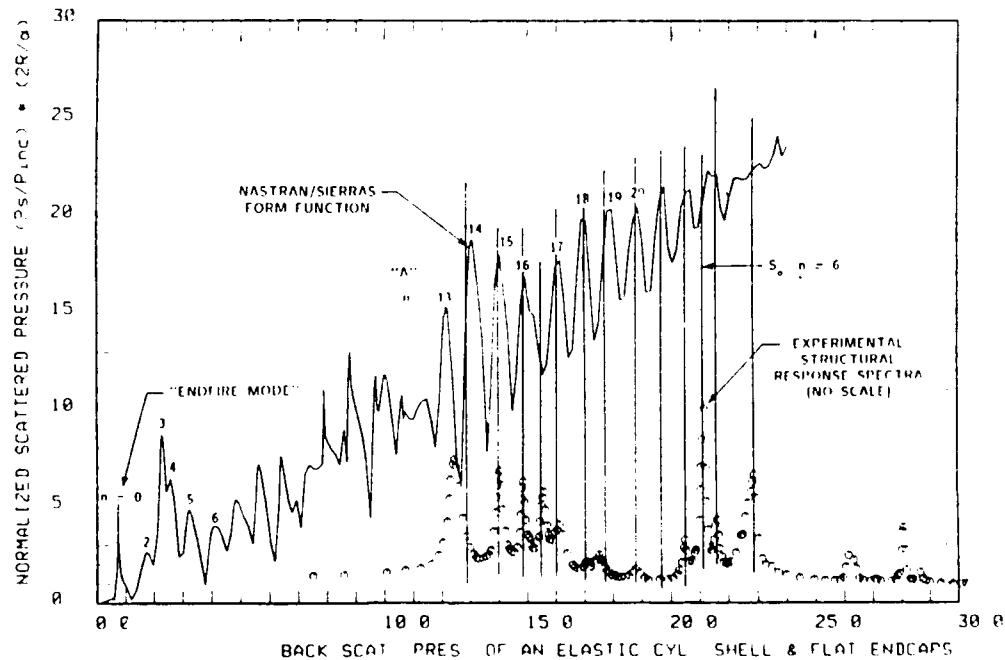
$ka=0.73$ $f=19.4$ Khz $n_{ENDCAP}=0$ node   (END FIRE MODE)
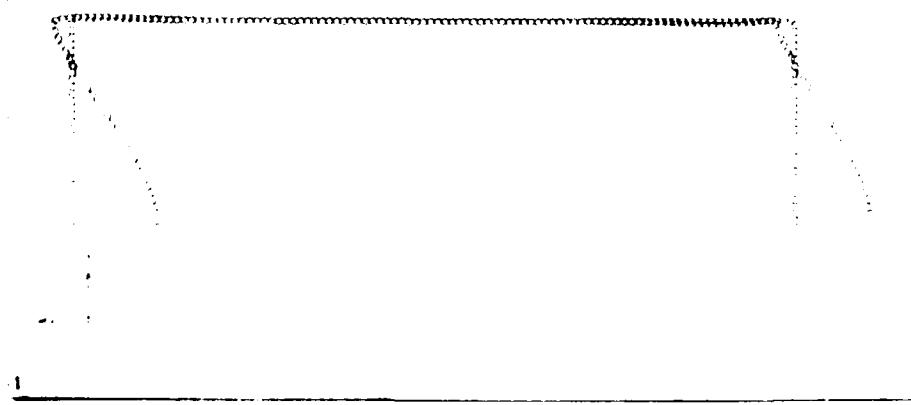
Fig. 8. NASTRAN/SIERRAS structural velocity response for the endfire resonance at ka = 0.73.

ka=19.8   f=524 Khz   n=20

1
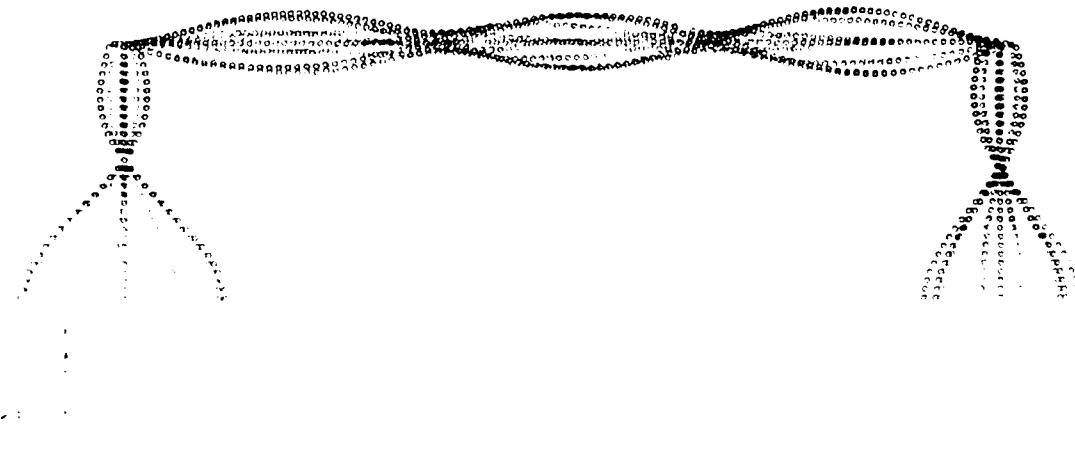
Fig. 9. NASTRAN/SIERRAS structural time progressive response for the
n = 3 cylindrical shell resonance at ka = 2.26.

1
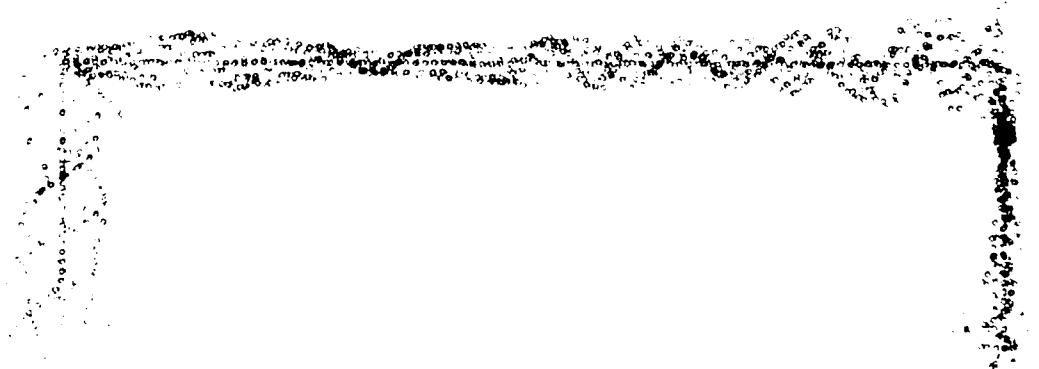
Fig. 10 NASTRAN/SIERRAS structural time progression response for the
n = 21 cylindrical shell resonance at ka = 19.8.
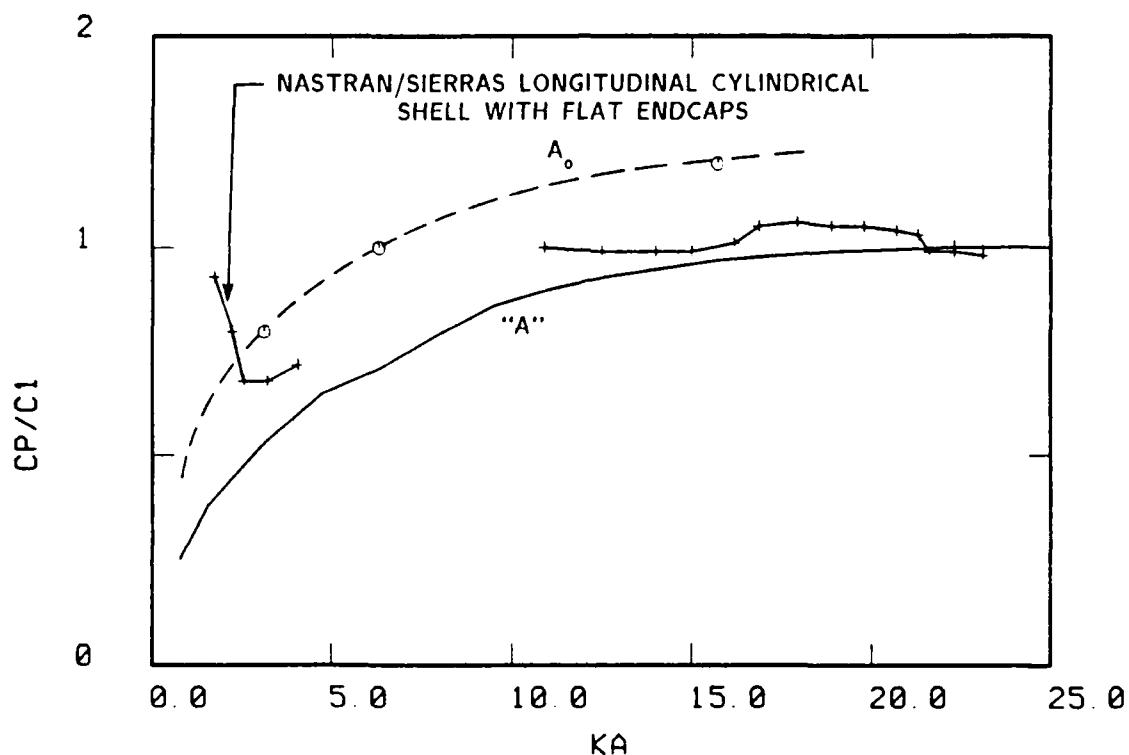
Fig. 11. Phase velocity dispersion curve for (Lamb-type) A_0 and A waves.